ResearchGate

See discussions, stats, and author profiles for this publication at: https://www.researchgate.net/publication/273557920

Relative Tropospheric Photolysis Rates of HCHO, H 13 CHO, HCH 18 O, and DCDO Measured at the European Photoreactor Facility

ARTICLE *in* THE JOURNAL OF PHYSICAL CHEMISTRY A · FEBRUARY 2007

Impact Factor: 2.69 · DOI: 10.1021/jp068794c

CITATIONS
3

READS
2

4 AUTHORS, INCLUDING:

Barbara D'Anna
French National Centre for Scientific Research
133 PUBLICATIONS **1,784** CITATIONS

SEE PROFILE

Matthew S Johnson
University of Copenhagen
138 PUBLICATIONS **1,683** CITATIONS

SEE PROFILE

Available from: Matthew S Johnson
Retrieved on: 22 January 2016

Relative Tropospheric Photolysis Rates of HCHO and HCDO Measured at the European Photoreactor Facility

Karen L. Feilberg,[†] Matthew S. Johnson,[†] Asan Bacak,[‡,§] Thomas Röckmann,[‡,§] and Claus J. Nielsen*[,||]

Copenhagen Center for Atmospheric Research, Department of Chemistry, University of Copenhagen, Universitetsparken 5 DK-2100 Copenhagen OE, Denmark, Max Planck Institute for Nuclear Physics, Atmospheric Physics Division, Saupfercheckweg 1, 69177 Heidelberg, Germany, Institute for Marine and Atmospheric Research Utrecht (IMAU), Princetonplein 5, 3584 CC Utrecht, PO Box 80000, 3508 TA Utrecht, The Netherlands, and Centre for Theoretical and Computational Chemistry, Department of Chemistry, University of Oslo, PO Box 1033 − Blindern 0315 Oslo, Norway

Received: January 9, 2007; In Final Form: July 4, 2007

The relative photolysis rates of HCHO and HCDO have been studied in May 2004 at the European Photoreactor Facility (EUPHORE) in Valencia, Spain. The photolytic loss of HCDO was measured relative to HCHO by long path FT-IR and DOAS detection during the course of the experiment. The isotopic composition of the reaction product H_2 was determined by isotope ratio mass spectrometry (IRMS) on air samples taken during the photolysis experiments. The relative photolysis rate obtained by FTIR is $j_{HCHO}/j_{HCDO} = 1.58 \pm 0.03$. The ratios of the photolysis rates for the molecular and the radical channels obtained from the IRMS data, in combination with the quantum yield of the molecular channel in the photolysis of HCHO, $\Phi_{HCHO\rightarrow H_2+CO}$ (*JPL Publication 06−2*), are $j_{HCHO\rightarrow H_2+CO}/j_{HCDO\rightarrow HD+CO} = 1.82 \pm 0.07$ and $j_{HCHO\rightarrow H+HCO}/(j_{HCDO\rightarrow H+DCO} + j_{HCDO\rightarrow D+HCO}) = 1.10 \pm 0.06$. The atmospheric implications of the large isotope effect in the relative rate of photolysis and quantum yield of the formaldehyde isotopologues are discussed in relation to the global hydrogen budget.

1. Introduction

Molecular hydrogen is the second most abundant reduced gas in the atmosphere, and its annual turnover in moles is larger than that of the most abundant reduced gas, methane. It has a lifetime of around 2[1−4] (and perhaps as little as 1.4)[5] years and is closely connected to the carbon cycle. About half of H_2 is produced by photolysis of formaldehyde, produced in turn by the oxidation of methane and non-methane hydrocarbons.[1,4,6,7] The photolysis of formaldehyde can proceed via two pathways at atmospherically relevant wavelengths:

$$HCHO + h\nu \rightarrow H + HCO \ (\lambda \leq 330 \text{ nm}) \qquad (1a)$$

$$HCHO + h\nu \rightarrow H_2 + CO \ (\lambda \leq 361 \text{ nm}) \qquad (1b)$$

The quantum yield of the two pathways depends on wavelength and thus varies throughout the atmosphere. Under average tropospheric conditions, the two photolysis pathways are of roughly equal importance.[8,9]

The oxidation of H_2 is an important source of water vapor in the stratosphere. Also, H_2 is an indirect greenhouse gas, since its addition to the atmosphere results in a decrease in the primary atmospheric oxidant OH and a corresponding increase in the greenhouse gas CH_4.[10] Several groups have investigated the environmental impact of H_2 in the recent past, in part because of the anticipated increase in the use of hydrogen fuel.[2,11−14] A conversion from a carbon-based to a hydrogen-based economy would have several consequences, including reduced emissions of NO_x, VOC, and CO_2, lower concentrations of tropospheric ozone, and an increase in stratospheric water vapor.[12]

The use of isotopic analysis has provided additional insight into many atmospheric systems.[15−17] Different trace gas sources often have different distinguishable isotopic signatures, and the removal processes are likewise associated with distinct fractionations for stable isotopes. Deuterium (D) isotope effects in particular are special due to the largest relative change in mass for any pair of stable isotopes of a single element. Two of the sources of atmospheric hydrogen, fossil fuel combustion and biomass burning, are depleted in D, having $\delta D(H_2)$ values of -196 ± 10 and -290 ± 60‰ respectively.[18] The processes removing molecular hydrogen are much slower for HD than for HH, with relative rates of 0.943 ± 0.024[18] and 0.595 ± 0.043[8,19,20] for soil uptake and OH reaction, respectively, and thus effectively enrich the remaining H_2 reservoir in the atmosphere. However, the fractionation in the removal process is not sufficient to explain the high deuterium content of tropospheric hydrogen of $\delta D(H_2) = 120 \pm 4$‰ (*versus* VSMOW, Vienna standard mean ocean water),[3,18] and according to present understanding hydrogen produced photochemically must acquire a D enrichment relative to the source material methane or isoprene. The value of $\delta D(CH_4)$ is -86 ± 3‰.[21] To the best of our knowledge no measurement of δD for plant isoprene has been made. However it is known that the biochemical synthesis of isoprenoids in plants produces compounds depleted in deuterium by hundreds of ‰.[22] The mechanism of the enrichment relative to precursors has yet to be demonstrated.

Formaldehyde, from which H_2 is produced via photolysis, is a key intermediate in the atmospheric oxidation of CH_4 and

* To whom correspondence should be addressed. c.j.nielsen@kjemi.uio.no.
† University of Copenhagen.
‡ Max Planck Institute for Nuclear Physics.
§ Institute for Marine and Atmospheric Research Utrecht.
|| University of Oslo.

10.1021/jp070185x CCC: $37.00 © 2007 American Chemical Society
Published on Web 08/24/2007

other hydrocarbons. Formaldehyde also reacts with OH, Cl, Br, $O(^1D)$, and NO_3: all these reactions are associated with kinetic isotope effects (KIEs) which can be used to distinguish the different reactions.[3,23] In most cases, the heavy isotopologue reacts more slowly with the radical species than the most abundant isotopologue leading to an enrichment of the heavy isotopologues in the remaining HCHO. We have previously shown that the formaldehyde reactions with OH, Br, Cl, and NO_3 radicals exhibit large hydrogen/deuterium fractionation constants ranging from 300‰ for Cl to 7500‰ for Br, whereas the ^{13}C fractionation constants are of the order of −48 (for the OH reaction) to +130‰ (for the Br reaction).[23−26] Likewise, the UV spectrum of formaldehyde is modified by isotopic substitution[27,28] and significant isotope effects in the tropospheric photolysis rates have been demonstrated.[29] The present work extends the studies of isotope effects in the photolysis of formaldehyde by addressing the central atmospheric HD source: HCDO.

2. Experimental Methods

2.1. Chemicals and Synthesis. The formaldehyde isotopologues used were in the form of paraformaldehyde, $(CH_2O)_n$. The HCHO sample was a commercial product from Fluka (extra pure); the monodeuterated formaldehyde was prepared in a 4-step synthesis ($HCBr_3 \rightarrow DCBr_3 \rightarrow HDCBr_2 \rightarrow HDC(OAc)_2 \rightarrow$ HCDO) as described previously;[30] the isotopic purity of the $(HCDO)_n$ product was determined by NMR to be 95.3%.

2.2. EUPHORE Experiments. The present experiments were carried out in the period May 24−28, 2004 in chamber A at the European Photoreactor Facility (EUPHORE) in Valencia, Spain (longitude −0.5, latitude 39.5). A detailed description of the EUPHORE facility and the existing analytical instruments is available in the literature,[31−35] and the present experiments are similar to those described in our recent report of the photolysis study of other formaldehyde isotopologues.[29] A typical experiment starts around 06:00 UT when reagents are added to the chamber. The canopy of the chamber is opened after a few FTIR spectra of the dark chamber have been recorded and the reagents are considered to be well-mixed. Depending on the photolysis rates of the reagents, the experiment lasts 2−4 h after which the chamber is closed and flushed overnight with scrubbed air. Typical variations in temperature, pressure, humidity, solar flux, j_{NO2}, $[O_3]$, [NO], $[NO_2]$, and [CO] in the chamber during an experiment are documented for May 26, 2004 in Figures S1−S9 (Supporting Information).

Approximately 100 mg of HCHO and 100 mg of HCDO were added to the ca. 200 m^3 chamber in each experiment by heating the paraformaldehyde polymer and flushing it into the chamber. The actinic flux (290−520 nm) was measured by a Bentham DM300 spectroradiometer throughout the experiment, DOAS spectra were recorded every 2 min and IR spectra were recorded every 15 min by co-adding 520 interferograms obtained at a resolution of 0.5 cm^{-1} (Nicolet Magna 550 FTIR spectrometer coupled with a White-type multi-reflection mirror system with an optical path length of 653.6 m). Unlike the typical laboratory smog chamber, purified air is constantly added to compensate for leakage, loss through connections and continuous sampling by ozone and NOx monitors. This is corrected for in the data analysis: SF_6 was added to measure the dilution rate. For each experiment, the analysis of the gas mixture was started at least 30 min before exposing the mixture to sunlight to check for dark reactions. The loss of formaldehyde in the dark was measured relative to that of SF_6. The results showed that any difference between the two losses was below the detection limit (ca. 1 ppb), indicating that no significant heterogeneous (including wall) reactions of formaldehyde are taking place.

Air samples for isotopic analysis of the H_2 product were taken at various times during the photolysis experiment. Approximately 8 L of air from the reaction chamber were compressed into 2 L volume electro-polished stainless steel flasks with a membrane compressor (Vacuubrand model ME 4P) through a drying trap filled with Drierite. Water could otherwise produce hydrogen on the metal surfaces. One or two background samples were taken in the dark reaction chamber before each experiment to establish the initial conditions.

The relative rate method was used to extract the relative photolysis rate of HCHO vs HCDO. The concentrations of the species undergoing photolysis are measured simultaneously as a function of reaction time. Consider two simultaneous photolysis processes with the rates j_{HCHO} and j_{HCDO}:

$$\mathrm{HCHO} + h\nu \xrightarrow{j_{HCHO}} \text{products}$$

$$\mathrm{HCDO} + h\nu \xrightarrow{j_{HCDO}} \text{products} \qquad (2)$$

Assuming that there are no loss processes other than these reactions and that there are no other processes producing the reactants, the following relation is valid:

$$\ln\left\{\frac{[\mathrm{HCHO}]_0}{[\mathrm{HCHO}]_t}\right\} = \frac{j_{HCHO}}{j_{HCDO}} \ln\left\{\frac{[\mathrm{HCHO}]_0}{[\mathrm{HCDO}]_t}\right\} \qquad (3)$$

where $[HCHO]_0$, $[HCHO]_t$, $[HCDO]_0$, and $[HCDO]_t$ denote the concentrations of the two isotopologues at times zero and t, respectively. A plot of $\ln([HCHO]_0/[HCHO]_t)$ vs $\ln([HCDO]_0/[HCDO]_t)$ will thus give the relative photolysis rate coefficient $\alpha = j_{HCHO}/j_{HCDO}$ as the slope, or in terms of the fractionation constant, $\epsilon = \alpha - 1$.

In the present case, however, three loss processes for the formaldehyde isotopologues in the chamber have to be taken into account − photolysis, reaction with OH, and dilution. In addition, there is a small HCHO production in the EUPHORE chamber, W_{HCHO}, which has been parametrized in terms of j_{NO2} and temperature.[36] Although the HCHO production in the chamber is small, ∼1 ppb h^{-1}, it is not negligible in the later part of the experiments. The concentrations of the isotopologues in the chamber can then be described by:

$$\frac{d[\mathrm{HCHO}]}{dt} = -(j_{HCHO} + k_{dilution} + k_{OH+HCHO}\cdot[OH])\cdot [\mathrm{HCHO}] + W_{HCHO}$$

$$\frac{d[\mathrm{HCDO}]}{dt} = -(j_{HCDO} + k_{dilution} + k_{OH+HCDO}\cdot[OH])\cdot [\mathrm{HCDO}] \qquad (4)$$

where $k_{dilution}$ is the dilution rate (see above), and $k_{OH+HCHO}$ and $k_{OH+HCDO}$ are the rate coefficients for the OH reaction with HCHO and HCDO, respectively. Although the actinic flux varies during the experiments, the daily variation is not large, Figure S4 (Supporting information). In addition, the variations are nearly proportional for the 300−400 nm region − the photoactive range for the two formaldehyde isotopologues. To a good approximation j_{HCHO} and j_{HCDO} will therefore have the same implicit time dependency, and the above equations may be solved to give the following relation:

$$\ln \frac{[\mathrm{HCHO}]_0}{[\mathrm{HCHO}]_t} - k_{\mathrm{dilution}} \cdot t - \int_0^t k_{\mathrm{OH+HCHO}} \cdot [\mathrm{OH}]_t \cdot \mathrm{d}t + \frac{\langle W \rangle}{[\mathrm{HCHO}]_0} \frac{\exp(\langle L \rangle \cdot t) - 1}{\langle L \rangle} = \frac{j_{\mathrm{HCHO}}}{j_{\mathrm{HCDO}}} \left(\ln \frac{[\mathrm{HCDO}]_0}{[\mathrm{HCDO}]_t} - k_{\mathrm{dilution}} \cdot t - \int_0^t k_{\mathrm{OH+HCDO}} \cdot [\mathrm{OH}]_t \cdot \mathrm{d}t \right) \quad (5)$$

in which we have introduced the loss rate coefficient for HCHO, $L = j_{\mathrm{HCHO}} + k_{\mathrm{dilution}} + k_{\mathrm{OH+HCHO}} \cdot [\mathrm{OH}]$, made use of $W(t)/[\mathrm{HCHO}]_0 \ll 1$, and because the time dependencies of L and W are complex but the functions well-behaved and bounded, approximated them by their average values during the experiment, $\langle L \rangle$ and $\langle W \rangle$. Typical values of $\langle L \rangle$ and $\langle W \rangle$ are around 1×10^{-4} s^{-1} and 5×10^{-4} ppb s^{-1}, respectively.

The dilution rate of the chamber, k_{dilution}, was determined for each experiment by adding ca. 20 ppb SF_6 gas to the chamber and monitoring its concentration by FTIR. The concentration of SF_6 was determined from the integrated intensity of its ν_3-(F_{1u}) band around 947.5 cm^{-1}:

$$\ln \{[\mathrm{SF_6}]_0/[\mathrm{SF_6}]_t\} = k_{\mathrm{dilution}} \cdot t \quad (6)$$

where $[SF_6]_0$ and $[SF_6]_t$ are the SF_6 concentrations at times zero and t, respectively. Typical values of k_{dilution} of the EUPHORE Chamber A during the present experiments are in the range of $3-4 \times 10^{-5}$ s^{-1}.

The concentrations of formaldehyde isotopologues as a function of time were extracted from the experimental infrared spectra by using a global FTIR nonlinear least-squares spectral fitting procedure developed by D. W. T. Griffith.[37] This method simulates the spectrum of the mixture of absorbing species from a set of initial concentrations and reference spectra and then varies the concentrations iteratively to minimize the residual between the measured and simulated spectrum. In the spectrum calculation, true absorption coefficients are used if available, otherwise high-resolution spectra can be used as a good approximation. The spectral features used in the analysis of the formaldehyde removal from the chamber were the C−H stretching bands of HCHO and HCDO in the 2670−2855 cm^{-1} region. The spectral data needed in the fitting procedure were taken from the HITRAN 2004 database (H_2O, CO, CO_2, CH_4);[38] for HCHO and HCDO experimental high-resolution IR spectra were used. The analysis of the FTIR spectra produced values for the relative change in concentrations which were subsequently analyzed according to eq 5 using a weighted least-squares procedure including uncertainties in both the "dependent" and "independent" variables.[39] The uncertainty assigned each data point includes a 5% relative error in the dilution contribution, a conservative estimate based on the fit to the SF_6 absorption features, a 10% relative error in the calculated loss due to reaction with OH radicals, estimated by considering possible limitations of the model, and a 30% relative error in the calculated HCHO source term, a conservative estimate.[36]

2.3. Reference Spectra. Infrared reference spectra of HCDO were recorded with a Bruker IFS 120 FTIR instrument at 0.01 cm^{-1} resolution in a 5 cm Pyrex gas cell equipped with CaF_2 windows. The partial pressure of formaldehyde was in the range 6−10 mbar and the cell was filled to 1013 mbar with synthetic air (Air Liquide, dry technical air). The gas cell was pretreated with ammonia before use to minimize the acid-catalyzed polymerization of the compound on the walls. A Ge on KBr beamsplitter and 1800−4000 cm^{-1} band-pass filter were used in the interferometer and a globar was used as the MIR light source. The detector was a liquid nitrogen (LN_2) cooled InSb semiconductor detector and 128 scans were co-added to achieve an acceptable signal/noise ratio in the resultant spectra. The reference spectra were placed on an absolute scale by fitting the absolute cross-sections of HCHO and HCDO recently obtained by Gratien et al. at 0.125 cm^{-1} resolution.[28]

2.4. HD/H_2 Analysis. The deuterium content of molecular hydrogen was determined on an analytical system based on the concept of Rhee et al.,[40] but including fully automated sample processing. A sample of ∼300 cm^3 of air is admitted to an evacuated sample volume where its pressure is determined within ±0.5 mbar. The bulk air and most trace gases are then condensed onto the cold head of a liquid helium compressor maintained at a temperature of ∼30 K, within 3 min. The gases remaining in the headspace are then flushed to a preconcentration trap using high-purity He at a flow rate of 20 cm^3 min^{-1}. The preconcentration trap is filled with molecular sieve (5 Å) and cooled to the triple point of nitrogen (63 K) by pumping the gas phase from a closed LN_2 Dewar system. The preconcentration trap is in the sample loop position of a 6-port sampling valve, and after preconcentration it is inserted into the analytical flow of ∼1.5 cm^3 min^{-1} He leading to the isotope ratio mass spectrometer. The trap is then lifted out of the LN_2 bath and heated to release the hydrogen. Nevertheless, desorption of hydrogen is not sufficiently fast to create a narrow peak, so the effluent from the preconcentration trap is concentrated again on the head of the molecular sieve analytical column immersed in liquid nitrogen. In this case the LN_2 temperature appears to be sufficient for quantitative trapping at the low flow rate used. To limit sample loss at the open split unit[41] the flow rate is decreased to ∼0.3 cm^3 min^{-1}, and the sample is sent through the column and via the open split into the mass spectrometer, where masses 2 and 3 are monitored simultaneously.

The new automated system has not yet been tested and calibrated as thoroughly as the previous manual system.[40] While isotopic reproducibility at typical atmospheric D concentrations is comparable to the original system (±3‰ in the δD value), the simultaneous measurement of the mixing ratio appears to be significantly worse. This is often related to large variations in the retention time of the peak and we suspect that it is due to limitations in the reproducibility of the mass flow controller that delivers the very low flow rate of 0.3 cm^3 min^{-1}. Additional effects may arise from incomplete trapping in the preconcentration or focusing traps, although no problems could be positively identified. Since this issue has not yet been resolved, reliable concentration measurements could not be obtained for the samples measured here. Fortunately however, the varying sample sizes do not compromise the isotope ratio, indicating that the loss process does not lead to isotopic fractionation. The measurements are put on the international scale using measurements of mixtures of H_2 with known isotopic composition in He or air and measurements of stratospheric air samples where the relation between its $\delta D(H_2)$ value and the mixing ratio of methane is precisely known. The former has the disadvantage that the analyzed mixtures are synthetic mixtures, the latter that it is not a very precise calibration. Both methods indicate an absolute offset of the raw data of 20 ± 20‰. Given the enormous enrichments that are measured in the samples, this does not produce a significant uncertainty. We have verified the absence of scale contraction using two isotope standards with an isotope difference of 214‰ (scale contraction <2%). Although the measured samples have much higher enrichments, isotope MS machines are highly linear and a stronger relative scale contraction at higher enrichments is not expected.

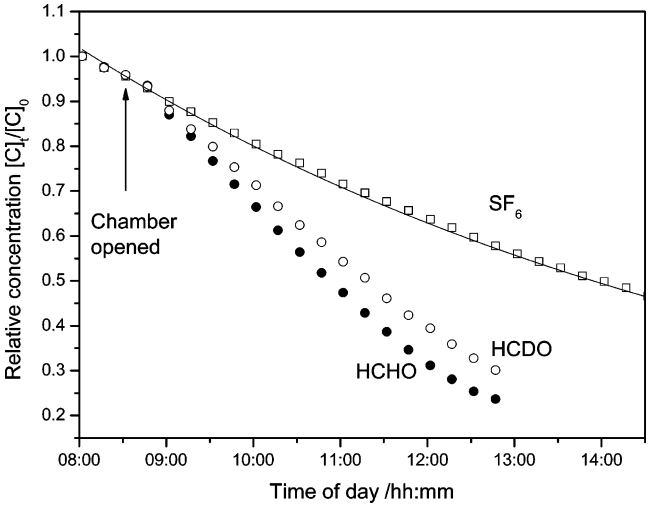

Figure 1. Relative concentration curves of SF_6 (□), HCHO (●), and HCDO (○) measured by FTIR during the photolysis experiment on May 26, 2004. The full curve corresponds to a constant dilution of $(3.35 \pm 0.04) \times 10^{-5}$ s^{-1}.

3. Results and Discussion

3.1. Relative Photolysis Rates. Figure 1 shows an example of normalized concentration curves of SF_6, HCHO, and HCDO obtained by FTIR during a photolysis experiment. There are clearly different rates of loss for HCHO and HCDO in addition to the dilution illustrated by the SF_6 concentration curve. OH radicals are formed in the chamber as hydrogen atoms and formyl radicals from the formaldehyde photolysis (eq 1) react with O_2 to generate HO_2 and eventually H_2O_2, OH, and O_3. As there is always a small amount of NO_x present, depending in part on outside conditions, these reactions could potentially generate enough OH that the OH + HCHO reaction would compete with photolysis, see Figures S7 and S8 (Supporting Information). It is obviously important to quantify the fraction of HCHO that reacts with OH as it is not only a loss process, but it is also associated with a kinetic isotope effect, which could influence the result.[23] The reaction system was therefore examined in a FACSIMILE kinetic model based on the Master Chemical Mechanism and specially designed for the EUPHORE chamber to elucidate the extent of the competing chemical reaction of HCHO with OH.[42] The model uses the temperature and the photolysis rate of NO_2 recorded in the chamber, and the initial concentrations of NO_x, O_3, and (in the present case) HCHO to simulate the OH concentration throughout the day for each of the experiments. The model includes an auxiliary OH chamber source determined in aromatic oxidation experiments.[42] The j_{NO2} values are used to scale the photolysis rates of all species in the model to match the specific conditions of a given day. Figure 2 shows the calculated OH concentration in the reaction chamber during an experiment: it may reach as much as 2×10^6 cm^{-3} in the middle of the day in some experiments and is used in the relative photolysis rate eq 5 to make the appropriate correction. The modeled loss rates of HCHO due to photolysis, dilution, OH reaction, as well as the wall source of HCHO are illustrated in Figure 3. In the example, the accumulated loss due to photolysis is around 66% of the total, dilution accounts for 27% of the total loss, the OH reaction for 7%, whereas wall production compensates for 3% of the total loss. The correction for dilution is large, but as the dilution rate is constant (and non-fractionating) throughout each experiment, the correction does not have a large effect on the accuracy of the result. In addition to generating OH radicals during the experiment, we also generate OD radicals. However, the total formaldehyde loss due to reaction with OH radicals is only around 7% of the total removal in all experiments. Further, there is a large labile hydrogen reservoir, around 50−70 ppm H_2O in the gas phase (Figure S3, Supporting Information) in addition to adsorbed surface water, and isotopic scrambling will effectively minimize the OD concentration. It is therefore irrelevant to distinguish between loss due to OH and OD in the present analyses.

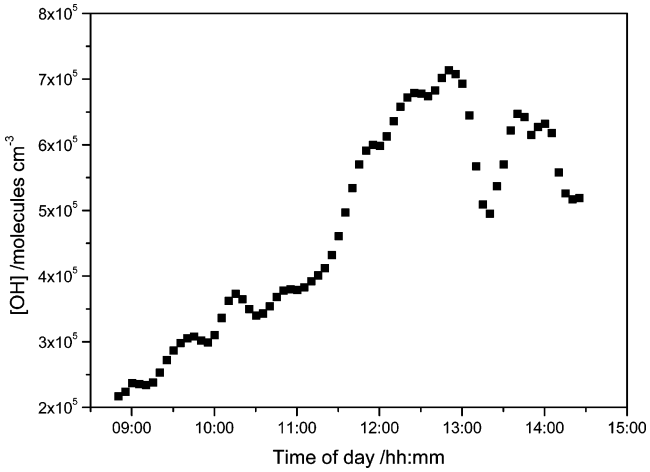

Figure 2. Calculated [OH] in the EUPHORE chamber A on May 26, 2004. See text for description of the model.

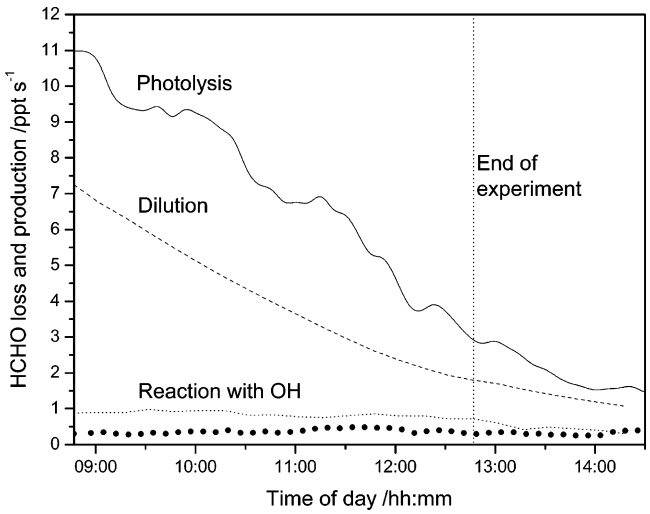

Figure 3. Loss and formation of HCHO in the EUPHORE chamber A during the photolysis experiment on May 26, 2004. The photolysis loss was calculated from the measured actinic flux, and the JPL recommended UV cross section and quantum yields.[8] The loss rate due to reaction with OH was calculated from a model of the chemistry in the chamber, see text. The wall production of HCHO (●) was calculated from the parametrization given in ref 36.

Figure 4 shows plots according to eq 5 of the HCHO and HCDO losses as measured by FTIR during the 5 experiments, whereas Figure 5 shows an example of the spectral fitting. The results from the weighted least-squares analyses are summarized in Table 1. The average relative photolysis rate $j_{rel} = j_{HCHO}/j_{HCDO}$ is 1.58 ± 0.03, where the quoted error represents 2σ from the statistical analysis. The larger variation between daily results seen in the DOAS measurements, Table 1, showed that technique was significantly less reliable than FTIR. The results from the analyses of the DOAS data vary with the initial HCHO and HCDO concentrations and much more from day to day than the FTIR results do. We therefore consider the present DOAS results as less reliable.

3.2. Relative Absolute and Channel-Specific Photolysis Rates. The photolysis quantum yields for HCHO have been

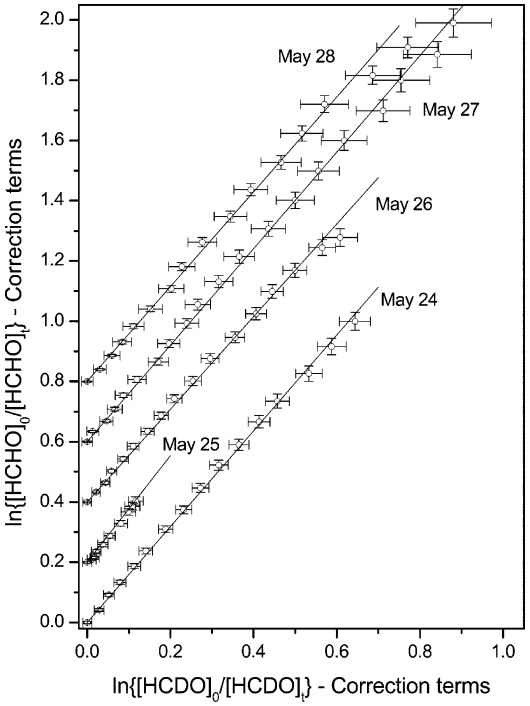

Figure 4. Relative concentration curves of HCDO versus HCHO during photolysis experiments in the EUPHORE reactor as measured by FTIR. The data shown are corrected for loss due to dilution and reaction with OH; error bars include the 1σ error from the spectral analysis and the estimated uncertainties in the correction terms given in eq 5. The average relative photolysis rate from 4 independent experiments is 1.58 ± 0.03 (2σ). Data offset by 0.2, 0.4, 0.6, and 0.8 for May 25−28, respectively.

the subject of several studies, and the results have been critically reviewed.[8] Similar results for other formaldehyde isotopologues have not been reported. Measurements of the HD/H_2 ratio in the chamber air as a function of time in the HCHO/HCDO experiments allow the values of the integrated quantum yield of HD for the tropospheric photolysis of HCDO to be estimated. Assuming (*i*) that diffusion of hydrogen into the chamber from the outside is insignificant and can be ignored and (*ii*) that the purified air added to compensate for loss (see Experimental Section) has a constant hydrogen content and isotopic signature equal to those at the start of the experiment, $[H_2]_0$ and $[HD]_0$, the differential rate laws describing H_2 and HD in the chamber air are:

$$\frac{d[H_2]}{dt} = k_{dilution}\cdot[H_2]_0 + j_{HCHO\rightarrow CO+H_2}(t)\cdot[HCHO] - k_{dilution}\cdot[H_2] - k_{OH+H_2}\cdot[H_2]\cdot[OH]$$

$$\frac{d[HD]}{dt} = k_{dilution}\cdot[HD]_0 + j_{HCDO\rightarrow CO+HD}(t)\cdot[HCDO] - k_{dilution}\cdot[HD] - k_{OH+HD}\cdot[HD]\cdot[OH] \quad (7)$$

where we have explicitly stressed that the photolysis rates, $j_{HCHO\rightarrow CO+H_2}$ and $j_{HCDO\rightarrow CO+HD}$, are time dependent. The photolysis rate of HCHO for CO + H_2 formation, $j_{HCHO\rightarrow CO+H_2}(t)$, is related to the quantum yield, $\Phi_{HCHO\rightarrow CO+H_2}$, the absorption cross section, $\sigma(\lambda)$, and the actinic flux, $F(\lambda,t)$:

$$j_{HCHO\rightarrow CO+H_2}(t) = \int \Phi_{HCHO\rightarrow CO+H_2}(\lambda)\cdot\sigma_{HCHO}(\lambda)\cdot F(\lambda,t)\cdot d\lambda = \varphi^{eff}_{HCHO\rightarrow CO+H_2}\cdot j^{abs}_{HCHO}(t) \quad (8)$$

where we have introduced an effective, integrated quantum yield, $\varphi^{eff}_{HCHO\rightarrow CO+H_2}$, and the absorption rate:

$$j^{abs}_{HCHO}(t) = \int \sigma_{HCHO}(\lambda)\cdot F(\lambda,t)\cdot d\lambda \quad (9)$$

As shown in Figure S4 of the Supplimentary Information, the spectral distribution does not change with the time of day during the experiment, whereas the spectral intensity does change. In a similar way, we define the effective, integrated quantum yield for HD formation in the photolysis of HCDO and relate this to $j^{abs}_{HCHO}(t)$ by introducing the ratio $Q = j^{abs}_{HCDO}(t)/j^{abs}_{HCHO}(t)$. The fine-structures of the rovibronic UV spectra of HCHO and HCDO are obviously different.[27] However, the main progressions in the spectra are due to the C−O stretching mode of the excited-state, which is nearly unaffected by H/D substitution.[43] Further, the integrated band intensity of an electronic ro-vibronic transition is unaffected by isotopic substitution. Thus, Q is expected to be close to unity and to show only a very small and negligible time dependence during the experiments:

$$j_{HCDO\rightarrow CO+HD}(t) = \int \Phi_{HCDO\rightarrow CO+HD}(\lambda)\cdot\sigma_{HCDO}(\lambda)\cdot F(\lambda,t)\cdot d\lambda = \frac{\varphi^{eff}_{HCDO\rightarrow CO+HD}\cdot j^{abs}_{HCDO}(t)}{j^{abs}_{HCHO}(t)}\cdot j^{abs}_{HCHO}(t) = \varphi^{eff}_{HCDO\rightarrow CO+HD}\cdot Q\cdot j^{abs}_{HCHO}(t) \quad (10)$$

Equation 7 may then be written:

$$\frac{d[H_2]}{dt} = k_{dilution}\cdot[H_2]_0 + \varphi^{eff}_{HCHO\rightarrow CO+H_2}\cdot j^{abs}_{HCHO}(t)\cdot[HCHO] - k_{dilution}\cdot[H_2] - k_{OH\,+\,HCDO}\cdot[H_2]\cdot[OH]$$

$$\frac{d[HD]}{dt} = k_{dilution}\cdot[HD]_0 + \varphi^{eff}_{HCDO\rightarrow CO+HD}\cdot Q\cdot j^{abs}_{HCHO}(t)\cdot [HCDO] - k_{dilution}\cdot[HD] - k_{OH+HCDO}\cdot[HD]\cdot[OH] \quad (11)$$

The UV absorption cross section and the quantum yield are known for HCHO,[8] and j_{HCHO}, $j^{abs}_{HCHO}(t)$, and $\varphi^{eff}_{HCHO\rightarrow CO+H_2}$ are readily calculated once the actinic flux is available. The reaction rate coefficients of OH with H_2 and HD are 6.7×10^{-15} and 4.0×10^{-15} $cm^3\ s^{-1}$, respectively.[8] Therefore, even with OH concentrations around 10^6 cm^{-3}, the loss rates of H_2 and HD due to reaction with OH will be less than 10^{-8} s^{-1}, which is several orders of magnitude less than the rates of dilution and formation by photolysis of formaldehyde and can thus be neglected.

The content of H_2 and HD in the chamber air is then modeled by numerical integration of eq 11 for comparison with the measurements:

$$[H_2]_{t+\Delta t} = [H_2]_t + (k_{dilution}\cdot([H_2]_0 - [H_2]_t) + \varphi^{eff}_{HCHO\rightarrow CO+H_2}\cdot j^{abs}_{HCHO}(t)\cdot[HCHO]_t)\cdot\Delta t$$

$$[HD]_{t+\Delta t} = [HD]_t + (k_{dilution}\cdot([HD]_0 - [HD]_t) + \varphi^{eff}_{HCDO\rightarrow CO+HD}\cdot Q\cdot j^{abs}_{HCHO}(t)\cdot[HCDO]_t)\cdot\Delta t \quad (12)$$

The concentrations of HCHO and HCDO, in turn, are modeled by eq 4 using the experimental values for $k_{dilution}$, j_{HCHO}, $j_{rel} = j_{HCHO}/j_{HCDO}$ and taking the OH concentrations from

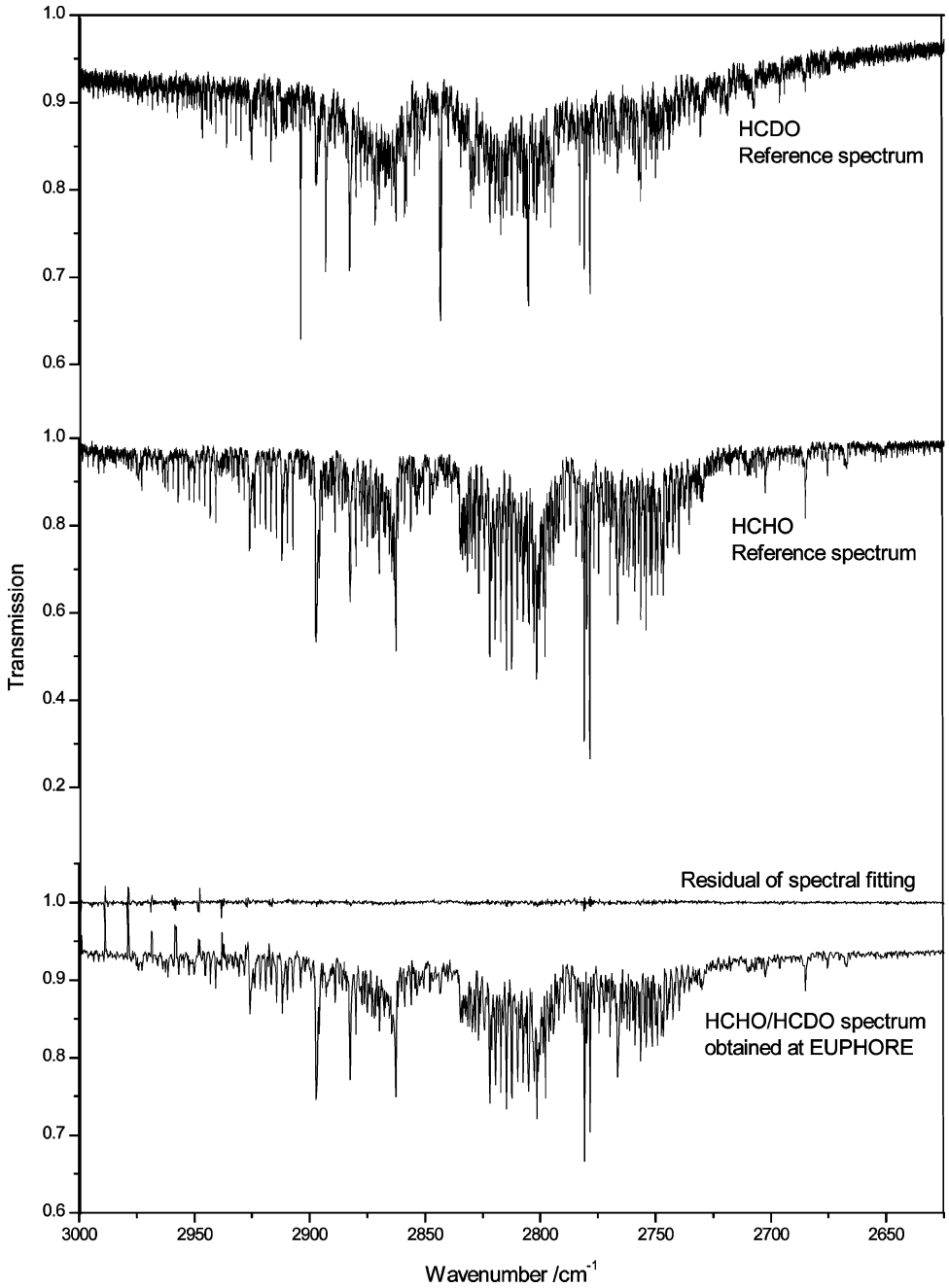

Figure 5. FTIR spectra of formaldehyde isotopologues. (Top) Reference spectrum of HCDO (res 0.02 cm^{-1}, 1 atm of N_2). Middle: Reference spectrum of HCHO (res 0.02 cm^{-1}, 1 atm of N_2). (Bottom) HCHO/HCDO mixture obtained at EUPHORE (res 0.5 cm^{-1}, 1 atm air) and the residual from spectral fitting.

TABLE 1: Summary of Relative Photolysis Rates Measured by FTIR on Five Consecutive Days[a]

			$J_{rel} = J_{HCHO}/J_{HCDO}$		
date of experiment	$[HCHO]_0/[HCDO]_0$ /ppb	$k_{dilution}$ /10^{-5} s^{-1}	FTIR	DOAS	$J_{HCHO\rightarrow CO+H2}/J_{HCDO\rightarrow CO+HD}$
24−05−2004	243/168	3.45 ± 0.04	1.59 ± 0.03	1.60 ± 0.06	1.85 ± 0.10
25−05−2004	240/162	3.25 ± 0.04	1.77 ± 0.20	−	−
26−05−2004	224 /182	3.35 ± 0.04	1.54 ± 0.04	1.50 ± 0.04	1.90 ± 0.12
27−05−2004	244/93	3.81 ± 0.04	1.60 ± 0.03	2.07 ± 0.04	1.80 ± 0.10
28−05−2004	275/81	3.53 ± 0.04	1.57 ± 0.05	1.72 ± 0.06	1.75 ± 0.10
Weighted average			1.58 ± 0.03	1.75 ± 0.15	1.82 ± 0.07

[a] Errors represent 2 sigma derived from the statistical analyses. Due to the onset of rain around noon, the result from May 25th is excluded from the analysis.

separate FACSIMILE simulations of the chamber chemistry (see above). Figure 6 illustrates the close agreement between observed and modeled HCHO and HCDO losses in the reactor as a function of time according to eq 4. Figure 7 shows the model results and experimental data for the isotopic composition of the reaction product, $\delta D(H_2)$. The model does not fit the

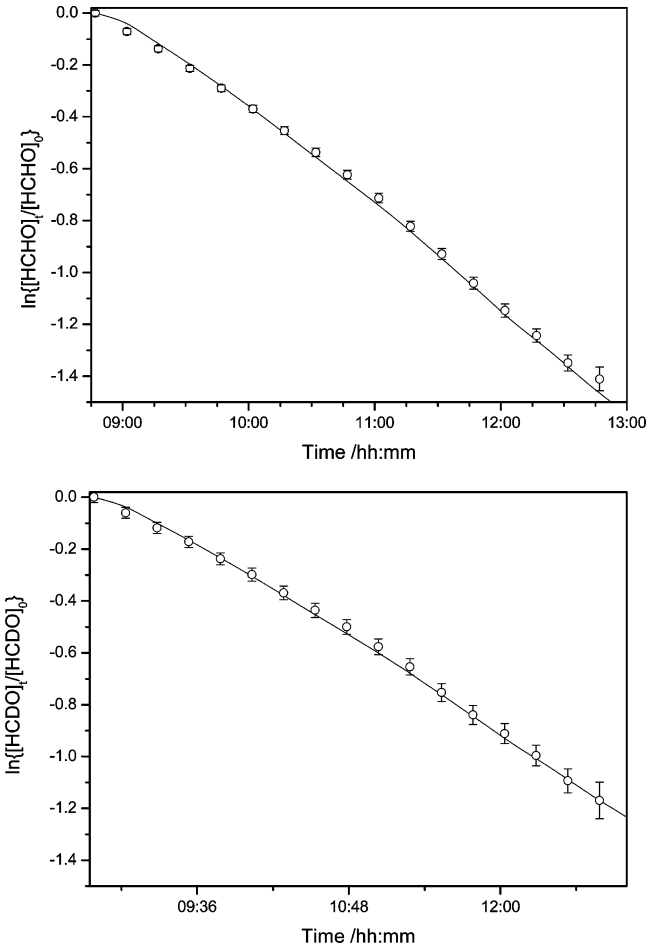

Figure 6. Observed and modeled loss of HCHO and HCDO in the EUPHORE Chamber A during photolysis, see text for description of the model. Data from May 26, 2004.

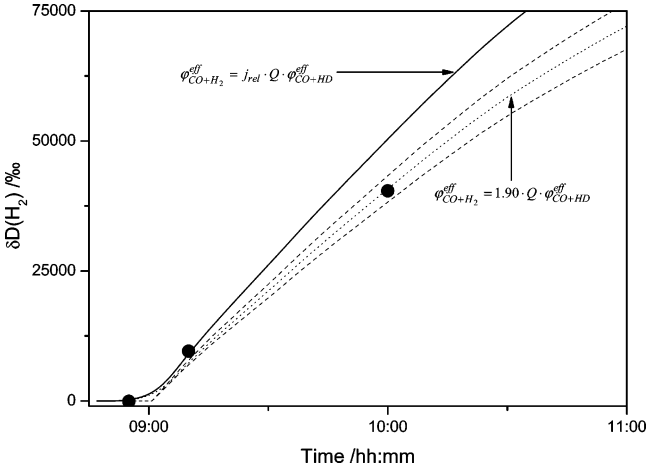

Figure 7. Observed and calculated $\delta D(H_2)$ in the EUPHORE Chamber A during photolysis of a HCHO/HCDO mixture, see text for description of the model. Data from May 26, 2004. (●) Measurements by isotope ratio mass spectrometry. The full curve corresponds to $j_{HCHO\rightarrow CO+H_2}/j_{HCDO\rightarrow CO+HD} = j_{rel} = 1.54$. The dotted curve corresponds to $j_{HCHO\rightarrow CO+H_2}/j_{HCDO\rightarrow CO+HD} = 1.90$. The dashed curves represent the estimated 1σ confidence interval. Results for the other days are shown in Figures S10−S12 (Supporting Information).

data when $\varphi^{eff}_{HCHO\rightarrow CO+H_2}/(Q\cdot\varphi^{eff}_{HCDO\rightarrow CO+HD})$ is set equal to j_{rel}. In this case the HD yield is far too high. This demonstrates that the effective quantum yield of the molecular channel in tropospheric HCHO photolysis must be significantly larger than j_{rel} times that of HCDO. In fact, the experimental data can be

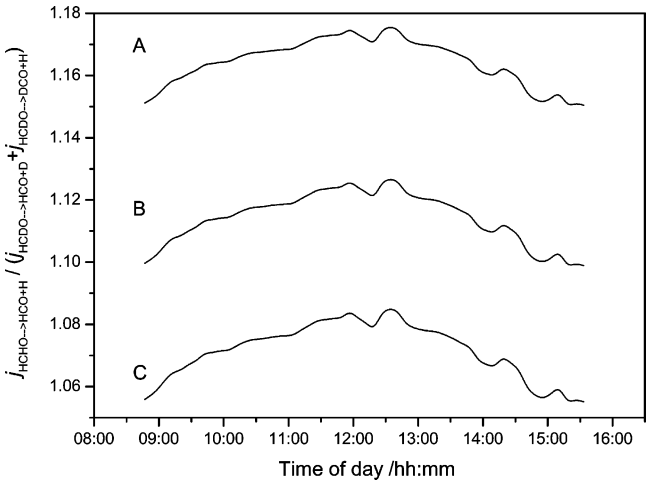

Figure 8. Calculated relative photolysis rate $J_{HCHO\rightarrow HCO+H}/(J_{HCDO\rightarrow HCO+D}+J_{HCDO\rightarrow DCO+H})$ as a function of time of day. Data from May 26, 2004. (A) $J_{HCHO\rightarrow HCO+H_2}/J_{HCDO\rightarrow CO+HD} = 1.75$, (B) $J_{HCHO\rightarrow HCO+H_2}/J_{HCDO\rightarrow CO+HD} = 1.82$, (C) $J_{HCHO\rightarrow HCO+H_2}/J_{HCDO\rightarrow CO+HD} = 1.89$.

reproduced well if $\varphi^{eff}_{HCHO\rightarrow CO+H_2}/(Q\cdot\varphi^{eff}_{HCDO\rightarrow CO+HD})$ is on the average 1.15 times higher than j_{rel} (Figure 7). The results for $j_{HCHO\rightarrow CO+H_2}/j_{HCDO\rightarrow CO+HD} = \varphi^{eff}_{HCHO\rightarrow CO+H_2}/(Q\cdot\varphi^{eff}_{HCDO\rightarrow CO+HD})$ from the analyses of the H/D content on the individual days of experiments are included in Table 1; data representations equivalent to Figure 7 for the other days are given in Figures S10−S12 (Supporting Information).

In the relation between the relative photolysis rate and the effective quantum yields, eq 13, the two terms in the nominator can be calculated from the recommended absorption cross-sections and photolysis quantum yields of HCHO[8] and the measured actinic flux:

$$j_{rel} = \frac{j_{HCHO}}{j_{HCDO}} = \frac{j_{HCHO\rightarrow CO+H_2} + j_{HCHO\rightarrow HCO+H}}{j_{HCDO\rightarrow CO+HD} + j_{HCDO\rightarrow HCO+D} + j_{HCDO\rightarrow DCO+H}}$$

$$= \frac{\varphi^{eff}_{HCHO\rightarrow CO+H_2} + \varphi^{eff}_{HCHO\rightarrow HCO+H}}{Q\cdot(\varphi^{eff}_{HCDO\rightarrow CO+HD} + \varphi^{eff}_{HCDO\rightarrow HCO+D} + \varphi^{eff}_{HCDO\rightarrow DCO+H})} \quad (13)$$

j_{rel} and the ratio $j_{HCHO\rightarrow CO+H_2}/j_{HCDO\rightarrow CO+HD} = \varphi^{eff}_{HCHO\rightarrow CO+H_2}/Q\cdot\varphi^{eff}_{HCDO\rightarrow CO+HD}$ have been determined in the present experiments. Rearranging eq 13, we may extract the ratio between the photolysis rates of the radical channels in the two isotopologues:

$$\frac{j_{HCHO\rightarrow HCO+H}}{j_{HCDO\rightarrow HCO+D} + j_{HCDO\rightarrow DCO+H}} = \frac{\varphi^{eff}_{HCHO\rightarrow HCO+H}}{Q\cdot(\varphi^{eff}_{HCDO\rightarrow HCO+D} + \varphi^{eff}_{HCDO\rightarrow DCO+H})}$$

$$= \frac{j_{rel}\cdot\frac{j_{HCHO\rightarrow CO+H_2}}{j_{HCDO\rightarrow CO+HD}}}{\frac{j_{HCHO\rightarrow CO+H_2}}{j_{HCDO\rightarrow CO+HD}}\cdot\left(1+\frac{j_{HCHO\rightarrow CO+H_2}}{j_{HCHO\rightarrow HCO+H}}\right) - j_{rel}\cdot\frac{j_{HCHO\rightarrow CO+H_2}}{j_{HCHO\rightarrow HCO+H}}} \quad (14)$$

The spectral intensity (but not the spectral distribution) varies through the experiment, Figure S4 (Supporting Informtion) and, consequently, so do the photolyses rates. Figure 8 shows plots

TABLE 2: Mechanism for the Production of Hydrogen in the Oxidation of Methane, Including Propagation of Deuterium

R1	$CH_4 + OH \rightarrow CH_3 + H_2O$
R2a	$CH_3D + OH \rightarrow CH_3 + HDO$
R2b	$CH_3D + OH \rightarrow CH_2D + H_2O$
R3	$CH_3 + O_2 + M \rightarrow CH_3O_2 + M$
R4	$CH_2D + O_2 + M \rightarrow CH_2DO_2 + M$
R5a	$CH_3O_2 + HO_2 \rightarrow CH_3OOH + O_2$
R5b	$CH_3O_2 + HO_2 \rightarrow O_2 + HCHO + H_2O$
R6a	$CH_2DO_2 + HO_2 \rightarrow CH_2DOOH + O_2$
R6b	$CH_2DO_2 + HO_2 \rightarrow O_2 + HCDO + H_2O$
R6c	$CH_2DO_2 + HO_2 \rightarrow O_2 + HCHO + HDO$
R7	$CH_3O_2 + NO \rightarrow CH_3O + NO_2$
R8	$CH_2DO_2 + NO \rightarrow CH_2DO + NO_2$
R9	$CH_3O + O_2 \rightarrow HCHO + HO_2$
R10a	$CH_2DO + O_2 \rightarrow HCHO + DO_2$
R10b	$CH_2DO + O_2 \rightarrow HCDO + HO_2$
R11	$HCHO \rightarrow$ particle
R12	$HCDO \rightarrow$ particle
R13	$HCHO + OH \rightarrow CO + H_2O + HO_2$
R14	$HCDO + OH \rightarrow$ products
R15a	$HCHO + h\nu \rightarrow CO + H_2$
R15b	$HCHO + h\nu \rightarrow HCO + H$
R16a	$HCDO + h\nu \rightarrow CO + HD$
R16b	$HCDO + h\nu \rightarrow$ radical channel
R17	$H_2 + OH \rightarrow H + H_2O$
R18	$HD + OH \rightarrow$ products
R19	$H_2 \rightarrow$ soil
R20	$HD \rightarrow$ soil

of $j_{HCHO\rightarrow HCO+H}/(j_{HCDO\rightarrow HCO+D}+j_{HCDO\rightarrow DCO+H})$ as a function of time of day for $j_{HCHO\rightarrow CO+H_2}/j_{HCDO\rightarrow CO+HD} = 1.75$, 1.82, and 1.89: the variation during the day is around 2% compared to the 4% propagated uncertainty in $j_{HCHO\rightarrow CO+H_2}/j_{HCDO\rightarrow CO+HD}$. The average value of the relative photolysis rate of the radical channels is $j_{HCHO\rightarrow HCO+H}/(j_{HCDO\rightarrow HCO+D}+j_{HCDO\rightarrow DCO+H}) = 1.10 \pm 0.06$. Assuming $Q = 1$, the ratio between the effective quantum yields of the radical channels in the two isotopologues is then also 1.10 ± 0.06. We stress that the resulting values for $j_{HCHO\rightarrow CO+H_2}/j_{HCDO\rightarrow CO+HD}$ and $j_{HCHO\rightarrow HCO+H}/(j_{HCDO\rightarrow HCO+D}+j_{HCDO\rightarrow DCO+H})$ depend on the recommended quantum yields for HCHO photolysis.[8]

McQuigg and Calvert[44] conducted a pioneering study of HCHO, DCDO, and HCDO photolysis and concluded that $\varphi_{HCHO\rightarrow CO+H_2} + \varphi_{HCHO\rightarrow HCO+H} \approx 1$ over the entire absorption band. For DCDO and HCDO, however, their experiments showed that the sums of the quantum yields were less than unity in the long wavelength region. In their analyses, they argued, based upon unimolecular rate theory, that the ratios of the quantum yields for photolysis ($\varphi_{HCHO\rightarrow CO+H_2}/\varphi_{HCHO\rightarrow HCO+H}$ and $\varphi_{DCDO\rightarrow CO+D_2}/\varphi_{DCDO\rightarrow DCO+D}$) should be equal. Their data for HCDO were more uncertain, but apparently, this ratio was nearly the same also in HCDO. The latter finding is clearly not in agreement with the present results.

3.3. Propagation of Deuterium through the Oxidation Chain of Methane in the Troposphere. The previous section shows how deuterated formaldehyde is photolyzed more slowly than the parent isotopologue, and that it produces much less molecular hydrogen. This may seem inconsistent with the facts, since it is known that overall deuterium must be enriched in the process converting CH_4 to H_2 in the atmosphere. The purpose of this section is to show how this is possible and how the depletion of deuterium in photolysis can work together with the other steps in the process to produce an overall enrichment.

The concentration of deuterium in hydrogen produced by the oxidation of methane in the atmosphere will depend on the concentration of deuterium in the methane, and on the rates of the photochemical reactions involved in the oxidation process, *cf* Table 2. As shown in Scheme 1, the oxidation process occurs in five stages involving the subsequent conversion of methane into CH_3, CH_3O_2, CH_3O, HCHO, and finally, H_2.

At the first stage in the oxidation process:

$$\frac{[CH_2D]}{[CH_3]} = c_1 \frac{[CH_3D]}{[CH_4]} \tag{15}$$

Similarly, at the second stage,

$$\frac{[CH_2DO_2]}{[CH_3O_2]} = c_1 c_2 \frac{[CH_3D]}{[CH_4]} \tag{16}$$

Continuing in this manner, for the entire process we may write:

$$\frac{[HD]}{[H_2]} = c_1\, c_2\, c_3\, c_4\, c_5 \frac{[CH_3D]}{[CH_4]} = c\, \frac{[CH_3D]}{[CH_4]} \tag{17}$$

Converting from concentrations to delta values using the hydrogen number n_H, $\delta D(H_2) = \alpha\ \delta D(CH_4)$ where $\alpha = c \times n_H(CH_4)/n_H(H_2)$. We will proceed to derive the values c_i and the value of c for the entire mechanism in terms of rate coefficients and concentrations. Methane is the longest lived of the species occurring in the mechanism, and its atmospheric concentration has achieved a steady state, approximately, because its atmospheric concentration of 1750 ppb is increasing by less than a percent per year.[10] The shorter-lived species will also be in a dynamic steady state because their rates of formation and loss are in balance. We will therefore use the steady state approximation in analyzing the mechanism. To illustrate the concept, the mass balance equation for the methyl radical states that $d[CH_3]/dt$ will be equal to the rates of production minus the loss rates (*cf* Scheme 1, Table 2) and in the steady state approximation $d[CH_3]/dt$ is set to zero:

$$\frac{d[CH_3]}{dt} = k_1[OH]\cdot[CH_4] + k_{2a}[OH]\cdot[CH_3D] - k_3[CH_3]\cdot [O_2]\cdot[M] = 0 \tag{18}$$

This equation can be solved for $[CH_3]$:

$$[CH_3] = \frac{k_1[OH]\cdot[CH_4] + k_{2a}[OH]\cdot[CH_3D]}{k_3[O_2]\cdot[M]} \tag{19}$$

The ratio of $[CH_4]$ to $[CH_3D]$ in the atmosphere is roughly 1800 to 1, so $k_1[OH][CH_4] \gg k_{2a}[OH][CH_3D]$, and we can make the approximation:

$$[CH_3] = \frac{k_1[OH]\cdot[CH_4]}{k_3[O_2]\cdot[M]} \tag{20}$$

We apply the same procedure to CH_2D:

$$\frac{d[CH_2D]}{dt} = k_{2b}[OH]\cdot[CH_3D] - k_4[CH_2D]\cdot[O_2]\cdot[M] = 0 \tag{21}$$

giving

$$[CH_2D] = \frac{k_{2b}[OH][CH_3D]}{k_4[O_2][M]} \tag{22}$$

From eqs 20 and 22 we get the ratio:

$$\frac{[CH_2D]}{[CH_3]} = \frac{k_{2b}[OH]\cdot[CH_3D]}{k_4[O_2]\cdot[M]} \frac{k_3[O_2]\cdot[M]}{k_1[OH]\cdot[CH_4]} = \frac{k_{2b}}{k_1}\frac{k_3}{k_4}\frac{[CH_3D]}{[CH_4]} \quad (23)$$

A similar procedure can be used on CH_3O_2 giving:

$$\frac{[CH_2DO_2]}{[CH_3O_2]} = \frac{k_{2b}}{k_1}\frac{k_3}{k_4}\frac{k_4}{k_3}\frac{\{k_5[HO_2] + k_7[NO]\}}{\{k_6[HO_2] + k_8[NO]\}}\frac{[CH_3D]}{[CH_4]} = \frac{k_{2b}}{k_1}\frac{\{k_5[HO_2] + k_7[NO]\}}{\{k_6[HO_2] + k_8[NO]\}}\frac{[CH_3D]}{[CH_4]} \quad (24)$$

Here we have introduced $k_5 = k_{5a} + k_{5b}$; this convention regarding the name of the rate of the overall process will be used throughout the following derivation. Considering the methoxy radical, one can derive:

$$\frac{[CH_2DO]}{[CH_3O]} = \frac{k_8[CH_2DO_2]\cdot[NO]}{k_7[CH_3O_2]\cdot[NO]}\frac{k_9[O_2]}{k_{10}[O_2]} = \frac{k_8k_9[CH_2DO_2]}{k_7k_{10}[CH_3O_2]} \quad (25)$$

Substituting eq 24 into eq 25,

$$\frac{[CH_2DO]}{[CH_3O]} = \frac{k_{2b}}{k_1}\frac{\{k_5[HO_2] + k_7[NO]\}k_8k_9}{\{k_6[HO_2] + k_8[NO]\}k_7k_{10}}\frac{[CH_3D]}{[CH_4]} \quad (26)$$

The penultimate step involves applying the steady state approximation to formaldehyde. Starting with the parent species HCHO,

$$\frac{d[HCHO]}{dt} = P_{HCHO} - L_{HCHO} = 0 \quad (27)$$

where the rate of production of formaldehyde is given by:

$$P_{HCHO} = k_{5b}[CH_3O_2]\cdot[HO_2] + k_{6c}[CH_2DO_2]\cdot[HO_2] + k_9[CH_3O]\cdot[O_2] + k_{10a}[CH_2DO]\cdot[NO] \quad (28)$$

We know that the second and fourth terms are minor compared to the first and third, because there is much less of the deuterated, relative to the parent, species. In addition, $k_9[CH_3O][O_2] \gg k_{5b}[CH_3O_2][HO_2]$. So,

$$P_{HCHO} = k_9[CH_3O]\cdot[O_2] \quad (29)$$

The loss of formaldehyde involves several terms:

$$L_{HCHO} = k_{11}[HCHO] + k_{13}[HCHO]\cdot[OH] + k_{15}[HCHO] \quad (30)$$

Inserting eq 28 and 30 into eq 27 and solving for [HCHO],

$$[HCHO] = \frac{k_9[CH_3O]\cdot[O_2]}{k_{11} + k_{13}[OH] + k_{15}} \quad (31)$$

The corresponding expression for HCDO is:

$$[HCDO] = \frac{k_{10b}[CH_2DO]\cdot[O_2]}{k_{12} + k_{14}[OH] + k_{16}} \quad (32)$$

Combining eq 31 and 32, and simplifying,

$$\frac{[HCDO]}{[HCHO]} = \frac{k_{10b}}{k_9}\frac{\{k_{11} + k_{13}[OH] + k_{15}\}}{\{k_{12} + k_{14}[OH] + k_{16}\}}\frac{[CH_2DO]}{[CH_3O]} \quad (33)$$

Substituting eq 26 into eq 33 yields:

$$\frac{[HCDO]}{[HCHO]} = \frac{k_{2b}}{k_1}\frac{\{k_5[HO_2] + k_7[NO]\}k_8k_{10b}}{\{k_6[HO_2] + k_8[NO]\}k_7k_{10}}\frac{\{k_{11} + k_{13}[OH] + k_{15}\}}{\{k_{12} + k_{14}[OH] + k_{16}\}}\frac{[CH_3D]}{[CH_4]} \quad (34)$$

Finally, applying the steady-state approximation to that part of the atmospheric molecular hydrogen reservoir which is produced by methane oxidation:

$$\frac{[HD]}{[H_2]} = \frac{[HCDO]k_{16a}}{[HCHO]k_{15a}}\frac{\{k_{17}[OH] + k_{19}\}}{\{k_{18}[OH] + k_{20}\}} \quad (35)$$

Substituting eq 34 into eq 35 gives:

$$\frac{[HD]}{[H_2]} = \frac{k_{2b}}{k_1}\frac{\{k_5[HO_2] + k_7[NO]\}k_8k_{10b}}{\{k_6[HO_2] + k_8[NO]\}k_7k_{10}}\frac{\{k_{11} + k_{13}[OH] + k_{15}\}}{\{k_{12} + k_{14}[OH] + k_{16}\}}\frac{k_{16a}}{k_{15a}}\frac{\{k_{17}[OH] + k_{19}\}}{\{k_{18}[OH] + k_{20}\}}\frac{[CH_3D]}{[CH_4]} \quad (36)$$

We can now summarize the values of each of the constants c_i. From eq 23 we have:

$$c_1 = \frac{k_{2b}}{k_1}\frac{k_3}{k_4} \quad (37)$$

From eq 24 and 37 we extract

$$c_2 = \frac{k_4}{k_3}\frac{\{k_5[HO_2] + k_7[NO]\}}{\{k_6[HO_2] + k_8[NO]\}} \quad (38)$$

Similarly, from eq 25 we can derive

$$c_3 = \frac{k_8k_9}{k_7k_{10}} \quad (39)$$

And from eq 33,

$$c_4 = \frac{k_{10b}}{k_9}\frac{\{k_{11} + k_{13}[OH] + k_{15}\}}{\{k_{12} + k_{14}[OH] + k_{16}\}} \quad (40)$$

Finally from eq 35,

$$c_5 = \frac{k_{16a}}{k_{15a}}\frac{\{k_{17}[OH] + k_{19}\}}{\{k_{18}[OH] + k_{20}\}} \quad (41)$$

The equations derived above under the assumption of photochemical steady state for the short-lived species allow an analysis of isotopic composition of hydrogen as it is transferred through the short- and long-lived reservoirs in the conversion sequence from methane to hydrogen.

3.4. Evaluation of the Fractionation Constants. To estimate the isotopic composition at each stage of the mechanism, it is useful to calculate the proportionality constants for some assumed conditions that are representative for the oxidation of methane in the troposphere as a whole. The temperature is determined by observing that the predicted maximum in the atmospheric OH concentration occurs at a pressure of 700 mbar.[45] This corresponds to an altitude of 2.6 km. Taking an

SCHEME 1: Diagram of the Methane Oxidation Mechanism[a]

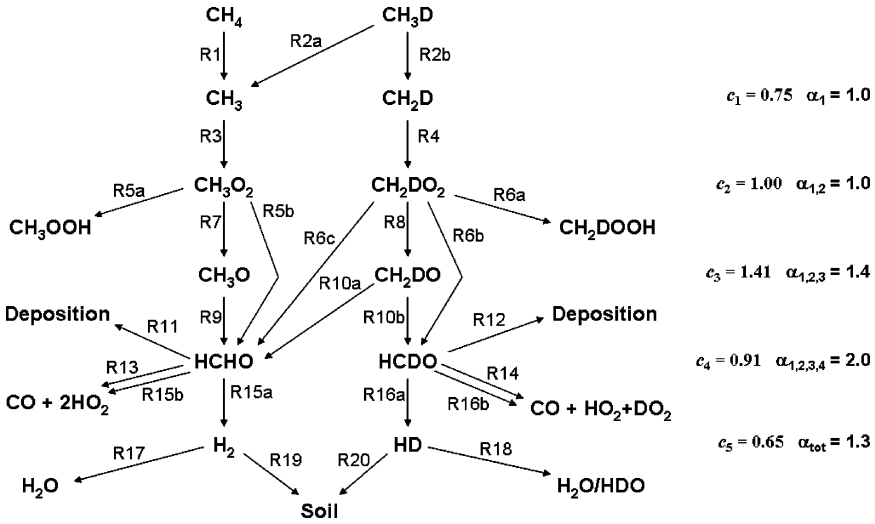

[a] The *c* values of the individual steps are shown along with the cumulative alpha values.

average surface temperature at the equator of 295 K and the lapse rate of the standard atmosphere of 6.5 K/km, the temperature at which CH_4 is most likely to be oxidized in the troposphere is about 280 K. Given this temperature and pressure, the number density of air is 1.81×10^{19} cm^{-3}.

3.4.1. The Methyl Radical, c_1. The proportionality constant for the first step depends on the rates k_1, k_{2b}, k_3, and k_4 as shown in eq 37. The rate of R2b (Scheme 1) is estimated by observing that the reactivity of the CH bond in CH_3D toward hydrogen abstraction by OH is nearly identical to that of the CH bond in CH_4;[46] using this argument, the rate for reaction R2b is $k_{2b} = (3/4) * k_1$.

k_{2a} does not enter into the expression for c_1. To the best of our knowledge, no measurements have been made concerning the absolute or relative rate of reaction of CH_2D with O_2 in R4. The deuterium atom is not directly involved in the reaction, and the isotope effect is expected to be small, and so we estimate that k_3 and k_4 are equal. Any error introduced by this approximation will cancel in the end, since c_1 depends on the ratio of k_3 to k_4 whereas c_2 depends on the ratio of k_4 to k_3. The final result is that $c_1 = 0.75$. In terms of delta values, $\delta D(CH_3) = \alpha_1 \times \delta D(CH_4)$ where $\alpha_1 = 4/3 \times c_1 = 1.0$.

3.4.2. The Methyl Peroxyl Radical, c_2. As shown in eq 38, the evaluation of c_2 involves the rates k_3, k_4, k_5, k_6, k_7, and k_8. The rates k_3 and k_4 were discussed above. Measurements of the absolute or relative rates of k_6 and k_8 are not available, however the deuterium atom is only a spectator in R6 and R8 (R6c is a minor channel), and so only secondary effects are expected. Therefore, the final result is that $c_2 = 1.00$, and because $n_H(CH_3) = n_H(CH_3O_2)$, α_2 is also estimated to be 1.00.

3.4.3. The Methoxy Radical, c_3. The evaluation of isotopic enrichment in the methoxy stage of the degredation of methane involves the rate coefficients k_7, k_8, k_9, and k_{10}. On the basis of the mechanism of the reaction, since only secondary isotope effects will take place, k_7 and k_8 will be set to be equal. Reactions R9 and R10 involve the abstraction of a hydrogen/deuterium atom from the methoxy radical, and therefore a large difference in reactivity is expected upon deuteration. In the abstraction of hydrogen/deuterium from methane, the C−H bond reacts 8 times faster than the C−D bond; applying this same ratio to k_9/k_{10}, one would expect a relative rate of 3*8/(2*8 + 1) because CH_3O has 3 C−H bonds and CH_2DO has 2 C−H bonds and one C−D bond. Therefore, using eq 44, the value of c_3 (equal to α_3) is estimated to be 1.41.

3.4.4. Formaldehyde, c_4. The rate of k_9 is 1.5×10^{-15} cm^{-3} s^{-1}.[8] The rate of k_{10b} can be calculated based on the arguments presented in the previous section to be 2/3 of k_9, that is, 1.0×10^{-15} cm^3 s^{-1}. The rates of deposition, photolysis and OH reaction for formaldehyde are highly variable, depending on local conditions. The rates of the photolysis and OH processes are approximately equal. The rate of the OH reaction (R13) is 8.7×10^{-12} cm^3 s^{-1},[8] which combined with a global average OH concentration of 1.2×10^6 cm^{-3} gives a zero-order rate constant for R13 of 1.0×10^{-5} s^{-1} or a lifetime of about a day. For the purpose of illustration, we will assign the same value to k_{15}. The rates of deposition of the formaldehyde isotopologues will be about equal, so $k_{12} = k_{11}$; initially, they will both be set to zero. However, in certain environments, the deposition rate will be significant. Therefore, we have also calculated the results for a deposition rate equal to the rates of photolysis and OH reaction (see below). The rate constant for the reaction of OH with HCDO in R14, k_{14}, is 78% as fast as that of HCHO in R13;[23] therefore, $k_{14} = 6.8 \times 10^{-12}$ cm^3 s^{-1}. As shown in the present study, the relative photolysis rate $j_{HCHO}/j_{HCDO} = 1.58$, so if k_{15} is 1.00×10^{-5} s^{-1}, then k_{16} is 6.76×10^{-6} s^{-1}. Combining all of this information in eq 40, the value of c_4 is estimated to be 0.94. In terms of fractionation constants $\alpha_4 = (3/2) \times c_4 = 1.41$.

3.4.5. Molecular Hydrogen, c_5. Equation 41 will be used to calculate c_5 based on k_{15a}, k_{16a}, k_{17}, k_{18}, k_{19}, k_{20}, k_{21}, and k_{22}. As reported in this paper, the ratio of k_{15a} to k_{16a} is 1.82. Using the JPL data compilation,[8] k_{17} is 4.3×10^{-15} cm^3 s^{-1} and k_{18} is 2.5×10^{-15} cm^3 s^{-1} at $T = 280$ K. According to Novelli et al.,[1] the rate of uptake of H_2 into the soil is three times that of the rate of loss through R17. Assuming the global average OH concentration is 1.2×10^6 cm^{-3}, this means that $k_{19} = 1.5 \times 10^{-8}$ s^{-1}. Gerst and Quay have measured the rate of uptake of HD into soil relative to H_2 as 0.943,[18] which combined with the estimate of k_{19} implies that $k_{20} = 1.4 \times 10^{-8}$ s^{-1}. Substituting these numbers into eq 41, one finds that c_5 is 0.65, and because $n_H(HCHO) = n_H(H_2)$, $\alpha_5 = c_5$.

3.4.6. Summary. The overall proportionality factor can be obtained from the product of the individual factors:

$$c = \prod_{i=1}^{5} c_i = 0.75 \times 1.00 \times 1.41 \times 0.94 \times 0.65 = 0.65 \quad (42)$$

TABLE 3: Global Isotope Budget of Hydrogen[a]

	term	strength /Tg a^{-1}	isotopic signature
sources	fossil fuel combustion	15 ± 10	-196 ± 10‰
	biomass burning	16 ± 5	-290 ± 60‰
	photochemical production	46 ± 19	185 ± 45‰ [b]
sinks	soil uptake	56 ± 41	0.943 ± 0.024
	OH oxidation	19 ± 9	0.606 ± 0.019
tropospheric burden	H_2	155 Tg	130 ± 4‰
	$(\sum S_i\delta_i/\sum S_i) - (\sum L_i\epsilon_i/\sum L_i)$		154

[a] From Gerst and Quay[18] except for photochemical isotopic signature, this work. [b] Assumes that δD(isoprene), which has not been measured, is the same as δD(methane).

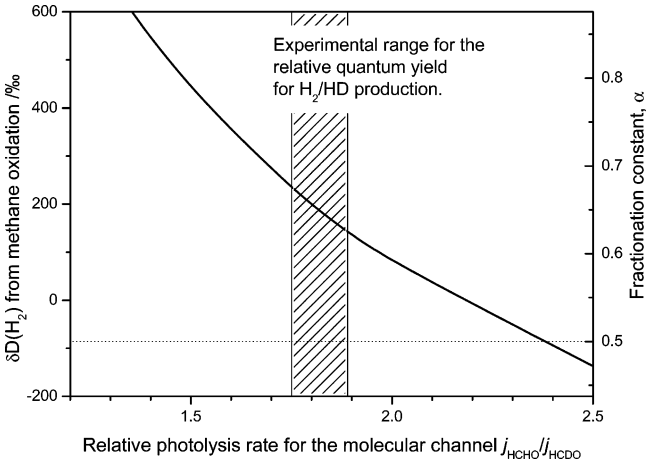

Figure 9. δD(H_2) from methane oxidation in the troposphere as a function of the relative quantum yield for H_2/HD production in the photolysis of HCHO and HCDO $j_{HCHO\rightarrow H2+CO}/j_{HCDO\rightarrow HD+CO}$. See text for description of the model.

This means that the ratio of deuterated to non-deuterated molecules in the H_2 product is approximately two-thirds as large as the one in the CH_4 substrate. In terms of fractionation constants $\alpha = (4/2) \times c = 1.3$, that is, according to the steady state approximation model, $\delta D(H_2) = 1.3 \times \delta D(CH_4)$.

3.5 Discussion. Scheme 1 summarizes the results of the calculation. It shows that the cumulative alpha value increases from 1.0 to 2.0 through the first four steps of the oxidation, and decreases to 1.3 at the final step. The reason that photolysis of formaldehyde can deplete deuterium in the hydrogen product without upsetting the overall budget is the extreme enrichment occurring in the steps leading up to its formation.

Several authors have investigated the isotopic budget of H and D in the stratosphere.[3,47,48] In addition to providing evidence for the isotopic signature of the *in situ* photochemical source of hydrogen in the absence of surface processes, this approach provides insight concerning stratospheric water vapor.[3,47−49] Stratospheric hydrogen is found mainly in three species: water, methane, and molecular hydrogen. At the tropical tropopause, δD(H_2) is 120‰. This delta value increases dramatically as air ages in the stratosphere, reaching values >400‰ at 30 km in mid latitudes and even lower altitudes in polar air. The δD(H_2) measurements show that stratospheric H_2 is by far the most deuterium-enriched hydrogen-containing compound found in natural materials on earth, only topped by some compounds found in unusual meteorites. Rahn and co-workers[3] derive a best fit value of $\alpha = 1.33$ for the rate of production of HD to H_2 in the oxidation process for methane in the stratosphere, based on stratospheric measurements and modeling. This would produce H_2 with $\delta D(H_2) = 215$‰ from tropospheric CH_4 (δD-(CH_4) = −86‰), whereas a value of $\delta D(H_2) = (180 \pm 50)$‰ was estimated for photochemical production at the tropopause with a similar box model.[47] The factor of $\alpha = 1.3$ derived in Section 3.4.6 is in good agreement with Rahn et al.'s value. In addition, Rhee et al. have modeled measurements of H_2, CH_4, $\delta D(H_2)$, and $\delta D(CH_4)$ in the stratosphere to obtain the relative oxidation rate for the stratosphere. This number was then adjusted for the troposphere by considering additional loss processes and changes in the actinic flux; they found a value of 1.30 ± 0.056, also in agreement with the result reported here.[50] In addition, the present results provide a mechanistic basis for understanding variations seen depending on location and time. For example, a recent study by Rice and Quay finds variation in δD(HCHO) between −296 and +210 for samples obtained in Seattle, Washington.[51]

Because $\delta D(CH_4)$ in the troposphere is −86‰, we have $[CH_3D]/[CH_4] = 5.70 \times 10^{-4}$. Using eq 17 and $c = 0.65$, we then get $[HD]/[H_2] = 3.7 \times 10^{-4}$. Finally, as $\delta = R_s/R_R - 1$, $\delta D(H_2)$ for photochemical hydrogen produced from methane, based on the experiments and discussion that has been presented here, is 185‰. The estimated error in $J_{HCHO\rightarrow CO+H2}/J_{HCDO\rightarrow CO+HD}$ places the lower and upper 2σ error limits in $\delta D(H_2)$ at 140 and 230‰, respectively. This is in fair agreement with the range of 130−230‰ derived from the stratospheric H_2 isotope data.[47] It should be emphasized that this interval reported here does not include the considerable uncertainties and approximations introduced in the steady state approximation model. The relation between the $\delta D(H_2)$ for photochemical hydrogen produced from methane and the relative yield for H_2/HD production in the tropospheric photolysis of formaldehyde, $J_{HCHO\rightarrow H2+CO}/J_{HCDO\rightarrow HD+CO}$, is shown in Figure 9.

The global isotope budget of hydrogen, adopted from Gerst and Quay,[18] is summarized in Table 3. Our steady-state model involves the kinetic isotope effects of many reactions and in some cases these were estimated, because they have not been determined in the laboratory, or investigated using theory. First, we have only considered methane as the tropospheric hydrogen precursor whereas in reality NMHC (mainly isoprene) oxidation accounts for an equal amount of hydrogen as methane does.[1,4,6,7] Second, the atmosphere is clearly much more complicated than Scheme 1, and in particular formaldehyde deposition could potentially have a large effect on isotopic enrichment. For example, the deposition velocity will be enhanced in the boundary layer and in the presence of particles. In a study of the formaldehyde chemistry above a forest canopy, Sumner and co-workers conclude that photolysis, dry deposition, and reaction with OH are equally important loss processes during the daytime in mid July to mid August:[52] this will obviously change δD-(H_2). To illustrate, if the rate of deposition of formaldehyde is set equal to the rates of photolysis and OH reaction, then c_4 decreases from 0.94 to 0.83 and c from 0.65 to 0.57. The result of increased deposition is to decrease the calculated $\delta D(H_2)$ by 140‰. To balance this non-fractionating loss the formaldehyde originating from isoprene oxidation has to be highly enriched in deuterium. As mentioned, there are at present no available measurements of the D-content in atmospheric isoprene. Stable

hydrogen isotope ratios of petroleum have been studied in detail. δD of crude oil ranges from −85 to −181‰[53] and one may argue that the D-content in emitted isoprene should be in this range. Terpenes used as flavorings show δD-values in the range from −230 to −330‰,[22] and one may equally well argue that isoprene should have a δD-value in this range. In any case, δD in isoprene is expected to be more depleted in deuterium than methane is, and the isotope fractionation in the isoprene oxidation processes must be huge to comply with the global $\delta D(H_2) = 130‰$. When all the reservations have been made, it is pleasing to see that the large deuterium isotope effects in the photolysis of formaldehyde obtained in the present experiments agree with the global hydrogen budget, Table 3.

4. Conclusions

Analysis of the oxidation process resolves the paradox of how HCDO can photolyze more slowly than HCHO and yield much less molecular hydrogen, and yet H_2 is enriched in D relative to the starting material, mainly methane and isoprene. The most important factor is the stability of the CD bond relative to CH. The first stages in the mechanism enrich D by up to ca. 1000‰, before D is depleted in photolysis.

In this paper, we have reported the first determination of the deuterium isotope effects in tropospheric photolysis of formaldehyde. Further, we have considered the impact of these isotope effects on atmospheric hydrogen. We have shown that factors such as deposition of formaldehyde will greatly influence the value of $\delta D(H_2)$ from tropospheric methane oxidation. Other factors that will clearly impact $\delta D(H_2)$ include the actual δD-(H_2) in isoprene as well as the deuterium fractionation in the isoprene oxidation processes, in addition to the details of the radical and irradiation fields, and temperature and pressure. Obviously, a detailed 3D model calculation of the global hydrogen isotope budget is needed to elucidate open issues such as the relative importance of formaldehyde deposition sink.

The relative photolysis rates j_{HCHO}/j_{HCDO}, $j_{HCHO\rightarrow CO+H2}/j_{HCDO\rightarrow CO+HD}$, and $j_{HCHO\rightarrow HCO+H}/(j_{HCDO\rightarrow HCO+D}+j_{HCDO\rightarrow DCO+H})$ are determined to be 1.58 ± 0.03, 1.82 ± 0.07 and 1.10 ± 0.06, respectively. Thus, the difference in the tropospheric photolysis rates of HCHO and HCDO lies mainly in the route for the molecular channel. It is by no means obvious that this should be so, and clearly, the UV cross-sections of HCDO and the quantum yields for HCDO photolysis should be studied in detail.

Acknowledgment. This work is part of the ACTION (Atmospheric Chemistry and Transport from Isotopic Analysis) project supported by the Norwegian Research Council. We acknowledge support from the Danish Natural Science Research Council and thank Juergen Schleucher for helpful discussions. We thank the anonymous reviewers for helpful comments.

Supporting Information Available: Typical variations in temperature (Figure S1), pressure (Figure S2), humidity (Figure S3), solar flux (Figure S4), j_{NO2} (Figure S5), $[O_3]$ (Figure S6), [NO] (Figure S7), $[NO_2]$ (Figure S8), and [CO] (Figure S9) in the EUPHORE chamber A during the experiments. Observed and calculated $\delta D(H_2)$ in the EUPHORE Chamber A during photolysis of HCHO/HCDO mixtures (Figures S10−S12). This material is available free of charge on the World Wide Web at http://pubs.acs.org.

References and Notes

(1) Novelli, P. C.; Lang, P. M.; Masarie, K. A.; Hurst, D. F.; Myers, R.; Elkins, J. W. *J. Geophys. Res., [Atmos.]* **1999**, *104*, 30427.

(2) Hauglustaine, D. A.; Ehhalt, D. H. *J. Geophys. Res., [Atmos.]* **2002**, *107*, 4330.

(3) Rahn, T.; Eiler, J. M.; Boering, K. A.; Wennberg, P. O.; McCarthy, M. C.; Tyler, S.; Schauffler, S.; Donnelly, S.; Atlas, E. *Nature* **2003**, *424*, 918.

(4) Sanderson, M. G.; Collins, W. J.; Derwent, R. G.; Johnson, C. E. *J. Atmos. Chem.* **2003**, *46*, 15.

(5) Rhee, T. S.; Brenninkmeijer, C. A. M.; Röckmann, T. *Atmos. Chem. Phys.* **2006**, *6*, 1611.

(6) Seiler, W.; Conrad, R. Contribution of tropical ecosystems to the global budgets of trace gases, especially CH_4, H_2, CO, and N_2O. In *The Geophysiology of Amazonia*; Dickinson, R. E., Ed.; John Wiley and Sons: New York, 1987; pp 133.

(7) Warneck, P. *Chemistry of the Natural Atmosphere*, 2nd ed.; Academic Press: New York, 1999.

(8) Sander, S. P.; Golden, D. M.; Kurylo, M. J.; Moortgat, G. K.; Wine, P. H.; Ravishankara, A. R.; Kolb, C. E.; Molina, M. J.; Finlayson-Pitts, B. J.; Huie, R. E.; Orkin, V. L. *Chemical Kinetics and Photochemical Data for Use in Atmospheric Studies*. Evaluation Number 15; National Aeronautics and Space Administration, Jet Propulsion Laboratory, California Institute of Technology: Pasadena, CA, 2006.

(9) Smith, G. D.; Molina, L. T.; Molina, M. J. *J. Phys. Chem.* A **2002**, *106*, 1233.

(10) IPCC "Climate Change 2001: The Scientific Basis. Contribution of Working Group I to the Third Assessment Report of the Intergovernmental Panel on Climate Change," Cambridge University Press, 2001.

(11) Rahn, T.; Eiler, J. M.; Kitchen, N.; Fessenden, J. E.; Randerson, J. T. *Geophys. Res. Lett.* 2002, *29*.

(12) Schultz, M. G.; Diehl, T.; Brasseur, G. P.; Zittel, W. *Science* **2003**, *302*, 624.

(13) Tromp, T. K.; Shia, R. L.; Allen, M.; Eiler, J. M.; Yung, Y. L. *Science* **2003**, *300*, 1740.

(14) Warwick, N. J.; Bekki, S.; Nisbet, E. G.; Pyle, J. A. *Geophys. Res. Lett.* **2004**, *31*.

(15) Johnson, M. S.; Feilberg, K. L.; von Hessberg, P.; Nielsen, O. J. *Chem. Soc. Rev.* **2002**, *31*, 313.

(16) Goldstein, A. H.; Shaw, S. L. *Chem. Rev.* **2003**, *103*, 5025.

(17) Brenninkmeijer, C. A. M.; Janssen, C.; Kaiser, J.; Röckmann, T.; Rhee, T. S.; Assonov, S. S. *Chem. Rev.* **2003**, *103*, 5125.

(18) Gerst, S.; Quay, P. *J. Geophys. Res., [Atmos.]* **2001**, *106*, 5021.

(19) Ehhalt, D. H.; Davidson, J. A.; Cantrell, C. A.; Friedman, I.; Tyler, S. *J. Geophys. Res., [Atmos.]* **1989**, *94*, 9831.

(20) Talukdar, R. K.; Gierczak, T.; Goldfarb, L.; Rudich, Y.; Rao, B. S. M.; Ravishankara, A. R. *J. Phys. Chem.* **1996**, *100*, 3037.

(21) Quay, P.; Stutsman, J.; Wilbur, D.; Snover, A.; Dlugokencky, E.; Brown, T. *Global Biogeochem. Cycles* **1999**, *13*, 445.

(22) Schmidt, H.-L.; Werner, R. A.; Eisenreich, W. *Phytochem. Rev.* **2003**, *2*, 61.

(23) Feilberg, K. L.; Johnson, M. S.; Nielsen, C. J. *J. Phys. Chem.* A **2004**, *108*, 7393.

(24) D'Anna, B.; Bakken, V.; Beukes, J. A.; Nielsen, C. J.; Brudnik, K.; Jodkowski, J. T. *Phys. Chem. Chem. Phys.* **2003**, *5*, 1790.

(25) Beukes, J. A.; D'Anna, B.; Bakken, V.; Nielsen, C. J. *Phys. Chem. Chem. Phys.* **2000**, *2*, 4049.

(26) Beukes, J. A.; D'Anna, B.; Nielsen, C. J. *Asian Chem. Lett.* **2000**, *4*, 145.

(27) Miller, R. G. *Photophysics of single vibronic levels in the* $\tilde{A}^1A_2$ state of *H_2CO, HDCO, and D_2CO*; University of California: Irvine, 1975.

(28) Gratien, A.; Nilsson, E.; Doussin, J.-F.; Johnson, M. S.; Nielsen, C. J.; Picquet-Varrault, B.; Stenstrøm, Y. *J. Phys. Chem.*, **2007**, submitted, jp074288r.

(29) Feilberg, K. L.; D'Anna, B.; Johnson, M. S.; Nielsen, C. J. *J. Phys. Chem.* A **2005**, *109*, 8314.

(30) Ouzounian, J. G.; Anet, F. A. L. *J. Labelled Compd. Radiopharm.* **1986**, *23*, 401.

(31) Becker, K. H. "The European Photoreactor EUPHORE. Design and Technical Development of the European Photoreactor and First Experimental Results," 1996.

(32) Magneron, I.; Thevenet, R.; Mellouki, A.; Le Bras, G.; Moortgat, G. K.; Wirtz, K. *J. Phys. Chem.* A **2002**, *106*, 2526.

(33) Volkamer, R.; Platt, U.; Wirtz, K. *J. Phys. Chem.* A **2001**, *105*, 7865.

(34) Klotz, B.; Sorensen, S.; Barnes, I.; Becker, K. H.; Etzkorn, T.; Volkamer, R.; Platt, U.; Wirtz, K.; Martin-Reviejo, M. *J. Phys. Chem.* A **1998**, *102*, 10289.

(35) Wenger, J. C.; Le Calve, S.; Sidebottom, H. W.; Wirtz, K.; Reviejo, M. M.; Franklin, J. A. *Environ. Sci. Technol.* **2004**, *38*, 831.

(36) Zador, J.; Turanyi, T.; Wirtz, K.; Pilling, M. J. *J. Atmos. Chem.* **2006**, *55*, 147.

(37) Griffith, D. W. T. *Appl. Spectrosc.* **1996**, *50*, 59.

(38) Rothman, L. S.; Jacquemart, D.; Barbe, A.; Benner, D. C.; Birk, M.; Brown, L. R.; Carleer, M. R.; Chackerian, C.; Chance, K.; Coudert, L. H.; Dana, V.; Devi, V. M.; Flaud, J. M.; Gamache, R. R.; Goldman, A.;

Hartmann, J. M.; Jucks, K. W.; Maki, A. G.; Mandin, J. Y.; Massie, S. T.; Orphal, J.; Perrin, A.; Rinsland, C. P.; Smith, M. A. H.; Tennyson, J.; Tolchenov, R. N.; Toth, R. A.; Vander Auwera, J.; Varanasi, P.; Wagner, G. *J. Quant. Spectrosc. Radiat. Transfer* **2005**, *96*, 139.

(39) York, D. *Can. J. Phys.* **1966**, *44*, 1079.

(40) Rhee, T. S.; Mak, J.; Röckmann, T.; Brenninkmeijer, C. A. M. *Rapid Commun. Mass Spectrom.* **2004**, *18*, 299.

(41) Röckmann, T.; Kaiser, J.; Brenninkmeijer Carl, A. M.; Brand Willi, A. *Rapid Commun. Mass Spectrom.* : RCM **2003**, *17*, 1897.

(42) Bloss, C.; Wagner, V.; Bonzanini, A.; Jenkin, M. E.; Wirtz, K.; Martin-Reviejo, M.; Pilling, M. J. *Atmos. Chem. Phys.* **2005**, *5*, 623.

(43) Sethuram. V.; Job, V. A.; Innes, K. K. *J. Mol. Spectrosc.* **1970**, *33*, 189.

(44) McQuigg, R. D.; Calvert, J. G. *J. Am. Chem. Soc.* **1969**, *91*, 1590.

(45) Wang, Y. H.; Jacob, D. J. *J. Geophys. Res., [Atmos.]* **1998**, *103*, 31123.

(46) Gierczak, T.; Talukdar, R. K.; Herndon, S. C.; Vaghjiani, G. L.; Ravishankara, A. R. *J. Phys. Chem.* A **1997**, *101*, 3125.

(47) Röckmann, T.; Rhee, T. S.; Engel, A. *Atmos. Chem. Phys.* **2003**, *3*, 2015.

(48) McCarthy, M. C.; Boering, K. A.; Rahn, T.; Eiler, J. M.; Rice, A. L.; Tyler, D. C.; Schauffler, S.; Atlas, E.; Johnson, D. G. *J. Geophys. Res., [Atmos.]* 2004, *109*.

(49) Zahn, A.; Franz, P.; Bechtel, C.; Grooss, J. U.; Röckmann, T. *Atmos. Chem. Phys.* **2006**, *6*, 2073.

(50) Rhee, T. S.; Brenninkmeijer, C. A. M.; Brass, M.; Bruhl, C. *J. Geophys. Res., [Atmos.]* 2006, *111*.

(51) Rice, A. L.; Quay, P. D. *Anal. Chem.* **2006**, *78*, 6320.

(52) Sumner, A. L.; Shepson, P. B.; Couch, T. L.; Thornberry, T.; Carroll, M. A.; Sillman, S.; Pippin, M.; Bertman, S.; Tan, D.; Faloona, I.; Brune, W.; Young, V.; Cooper, O.; Moody, J.; Stockwell, W. *J. Geophys. Res., [Atmos.]* **2001**, *106*, 24387.

(53) Yeh, H.-W.; Epstein, S. *Geochim. Cosmochim. Acta* **1981**, *45*, 753.